



GEOQuébec  
2015

Challenges from North to South  
Des défis du Nord au Sud

# A practical constitutive model for sands

Alireza Azami, Thamer Yacoub

Rocscience Inc., Toronto, Ontario, Canada

John Curran

Rocscience Inc. and Civil Engineering, University of Toronto, Toronto, Ontario, Canada

## ABSTRACT

This paper will focus on the behaviour of granular materials under monotonic loads and presents a constitutive model that is simple yet practical for engineering applications. The model is based on the well-known Mohr-Coulomb model with only one additional material parameter to make it as simple and practical as possible. The applicability of the model is demonstrated by simulations of triaxial tests, and various model tests, including strip foundation and tunnels with and without nearby surface load and also an excavation benchmark case study.

## RÉSUMÉ

Ce document se concentre sur le comportement des matériaux granulaires sous des charges monotones et présente un modèle constitutif simple, mais pratique pour les applications d'ingénierie. Ce modèle est basé sur le critère bien connu de Mohr-Coulomb. Seule l'addition d'un paramètre de matériau est effectuée afin de le rendre aussi simple et pratique que possible. L'application de ce dernier est démontrée par des simulations de tests triaxiaux, ainsi que divers tests de modèles, incluant la bande de fondations et les tunnels avec et sans charge de surface à proximité, ainsi qu'une étude de cas concernant l'excavation de référence.

## 1 INTRODUCTION

This paper will focus on the typical behaviour of granular materials under monotonic loads and presents a constitutive model that is simple yet practical for engineering applications. The behaviour of granular materials, more specifically sands, is usually studied under triaxial stress state in drained and undrained conditions. Under drained triaxial setup, for loose sands an increase in deviatoric strain is associated with hardening and progressive compaction, and as the deviatoric stress increases and stress state approaches the failure condition the volume change tends to zero. Dense sands show similar hardening behaviour up to a peak point or failure which is typically associated with formation of shear band and strain-softening behaviour. In dense sands at the initial stage of the deformation process the material undergoes compaction, and then at some point a transition from compaction to dilation occurs (Figure 1). The undrained behaviour typically is such that the compaction and dilation in the drained condition result in the generation of positive and negative pore pressure in the sample. The generation of excess pore water pressure in very loose sands can lead to liquefaction of the material. On the other hand, because of the generation of negative pore water pressures, very dense sands can endure high levels of deviatoric stress as illustrated in Figure 2 (e.g. Pietruszczak 2010).

The most common constitutive model in geotechnical engineering practice is the Mohr-Coulomb model. In addition to the elastic properties, three additional material properties, i.e. cohesion ( $c$ ), friction angle ( $\phi$ ) and dilation angle ( $\psi$ ) are required. The evaluation of these parameters, especially the friction angle and cohesion, is a common practice. The proposed constitutive model in this paper is based on the Mohr-Coulomb model with only one additional parameter and a new optional definition for the plastic flow.

The following sections will present the formulation of this constitutive model, explain the procedure to evaluate its parameters, and demonstrate its applicability in simulations of triaxial tests, and model tests. To further investigate the practicality of the model for engineering practice a well-documented benchmark problem that has been simulated by other researchers and commercialized geotechnical software, has been analyzed with the proposed model and a comparison between the numerical results and field observations is presented.

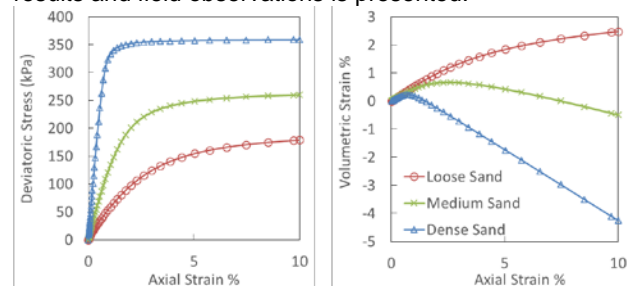


Figure 1. Example of the behaviour of loose, medium and dense sands in drained triaxial compression tests

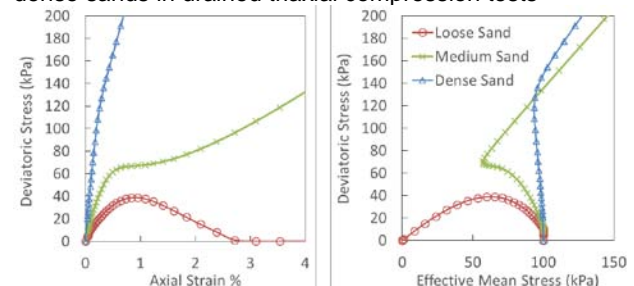


Figure 2. Example of the behaviour of loose, medium and dense sands in undrained triaxial compression tests

## 2 FOMULATION AND SPECIFICATION

In this section the formulation of this simple yet practical constitutive model will be presented. Comments will be made on the identification of material properties.

The most common constitutive model in soil mechanics and its engineering practice is the Mohr-Coulomb model. The proposed model is essentially based on this model and uses the same main material properties.

The equation for the Mohr-Coulomb yield surface using the  $(p, q, \theta)$  invariants is (e.g. Pietruszczak 2010)

$$F = q - M \left( p + \frac{c}{\tan \varphi} \right) = 0 \quad [1]$$

where the parameter  $M$  is the slope of the failure line in  $p - q$  plane and is defined as

$$M = \frac{3 \sin \varphi}{\sqrt{3} \cos \theta - \sin \theta \sin \varphi} \quad [2]$$

The additional concept in the proposed model is the notion of deviatoric hardening. Experimental evidence indicates that the plastic deformation in soils starts from the early stages of loading. To capture such behaviour in a constitutive model the typical elasto-perfect plastic models, such as the Mohr-Coulomb model, are not adequate. To simulate such behaviour constitutive models that utilize a hardening law after initial yielding are required. The hardening in the proposed model is considered for the mobilized friction angle and it is attributed to plastic distortion. The equations above are then rewritten as:

$$F = q - M \left( p + \frac{c}{\tan \varphi_f} \right) = 0 \quad [3]$$

$$M = \frac{3 \sin \varphi_m}{\sqrt{3} \cos \theta - \sin \theta \sin \varphi_m} \quad [4]$$

where  $\varphi_f$  is the friction angle at failure and  $\varphi_m$  is the mobilized friction angle.

The use of hyperbolic functions for describing the behaviour of soils has a long history in soil mechanics, for example the well-known Duncan-Chang model applies a hyperbolic function in its formulations (Duncan and Chang 1970). On this basis, the hardening rule in the proposed model for the mobilized friction angle takes advantage of a hyperbolic function:

$$\tan \varphi_m = \tan \varphi_f \frac{\varepsilon_q^p}{A + \varepsilon_q^p} \quad [5]$$

where  $\varepsilon_q^p$  is the plastic deviatoric strain and  $A$  is a constant hardening parameter. The hardening parameter is the only additional parameter in this model.

The plastic potential needs to be modified from its original form in the Mohr-Coulomb model. The formulation

used here takes advantage of the same idea of a dilation angle but assumes a constant ratio of the dilation angle to mobilized friction angle. Assuming a dilation angle at failure ( $\psi_f$ ) corresponding to the friction angle at failure this means:

$$\frac{\psi}{\varphi_m} = \frac{\psi_f}{\varphi_f} \quad [6]$$

In most cases under deviatoric loading stress paths the initial volumetric behaviour is compressive. In such cases the flow rule in equation 6 is not accurate. For such cases a flow rule similar to that proposed by Rowe (1962) should be utilized. For the proposed plastic potential, where the mobilized friction angle is less than the critical friction angle ( $\varphi_{cv}$ ) the volumetric behaviour is compressive, otherwise the volumetric behaviour is dilative. This type of flow rule can be captured by a plastic potential function defined in equations 7 and 8.

$$Q = q - M_{cv} p \ln(p/p_c) = const. \quad [7]$$

$$M_{cv} = \frac{3 \sin \varphi_{cv}}{\sqrt{3} \cos \theta - \sin \theta \sin \varphi_{cv}} \quad [8]$$

The plastic potential function is defined by a single parameter, the failure dilation angle or the critical friction angle, and this can be considered as a simple but useful modification to original plastic potential of the Mohr-Coulomb model.

Identification of all the model parameters are quite straightforward except for the hardening parameter  $A$ . The hardening parameter should be evaluated from curve fitting. The hardening parameter can be determined by plotting the tangent of mobilized friction angle versus the deviatoric strain obtained from experiments, and using equation 5 to find the best fit curve to these data points. The tangent of mobilized friction angle can be calculated based on the assumption that under a monotonic deviatoric loading, the material undergoes continuous yielding. Thus at every point on the stress path the state of stress is on the yield surface, and for each point the mobilized friction angle can be calculated from equations 3 and 4. For the purpose of this curve fitting it is assumed that the elastic strains are negligible compared to the plastic strains. Therefore, the plastic deviatoric strain is approximately equal to the total deviatoric strain,  $\varepsilon_q^p \approx \varepsilon_q$ .

As an example, Figure 3 shows this procedure for loose Hostun sand. As discussed later, the experimental points are from three different drained triaxial test conducted at confining pressure of  $\sigma_3 = 300$  kPa. In general parameter

$A$  is approximately 10% of the deviatoric strain at failure.

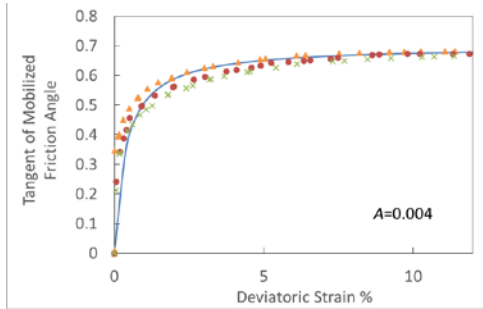


Figure 3. Evaluation of hardening parameter for loose Hostun sand

### 3 EXAMPLES

In this section the proposed constitutive model is used in simulations of some element tests, model tests and actual geotechnical structures to demonstrate and validate its capabilities. The model has been implemented in the finite element package RS<sup>2</sup> (Rocscience 2015).

#### 3.1 Drained and Undrained Triaxial Tests

The typical stress paths shown in Figures 1 and 2 are generated using the proposed constitutive model. Under drained conditions, the model is able to capture the hardening behaviour of sands and capture the volumetric compaction in loose sands and the compaction followed by dilation in dense sands. Under undrained condition the model can predict the static liquefaction of very loose sands, and can predict the generation of negative excess pore water pressure in dense sands. To better demonstrate these abilities simulations of some actual experimental data are presented in this section.

The experimental results of drained triaxial test on dense and loose Hostun sand are depicted from Schanz and Vermeer (1996).

Figure 4 shows the behaviour of loose Hostun sand in triaxial tests under confining pressure of  $\sigma_3 = 300$  kPa.

The figures include the results from 3 tests (data points) and numerical results generated by the proposed model (solid line). The simulated results are in good agreement with experimental observations in the prediction of hardening behaviour and volumetric compaction. The material properties used for this simulation is included in the graphs. Similarly, Figure 5 shows the behaviour of dense Hostun sand in drained triaxial tests.

Clearly the model is capable of capturing both the hardening and volumetric behaviour features. The post peak behaviour that is observed for dense Hostun sand is typically the result of development of a shear-band in the sample and is not to be considered as the material behaviour. In general, the softening behaviour observed in experiments is not the actual material behaviour, rather it is usually the result of development of some mechanism such as shear-banding. The proposed model here is only designed to capture the material behaviour that is associated with hardening. Extension to the softening branch requires more sophisticated formulations that can handle issues such as strain localization and development and propagation of shear bands.

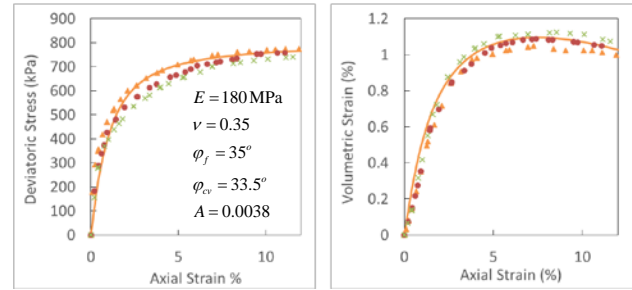


Figure 4. Drained triaxial test on loose Hostun sand

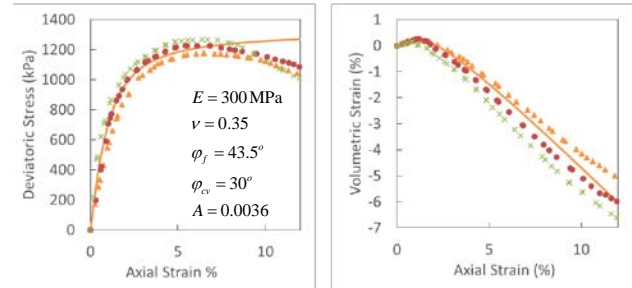


Figure 5. Drained triaxial test on dense Hostun sand

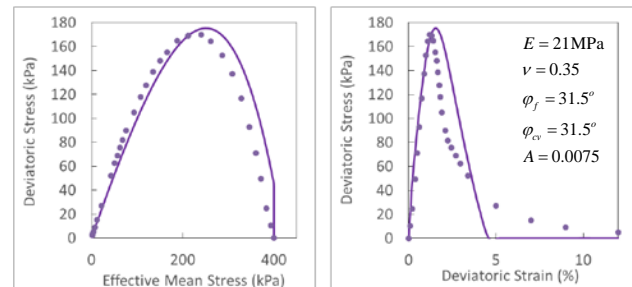


Figure 6. Undrained triaxial test on loose Banding sand

The undrained behaviour of loose Banding sand (Castro 1969) is presented in Figure 6. The triaxial test starts at the initial confinement of 400 kPa. The generation of excess pore water pressure in loose sands under undrained conditions can lead to static liquefaction and total loss of strength. This phenomenon can be observed in Figure 6. The simulation results presented in this figure are in good agreement with the experimental results.

#### 3.2 Model Test Simulations

The experimental results, including element and model tests results, in this section are from the research work by Shahin et.al (2011) and Nakai (2013). The material used to model the soil consists of a mix of 1.6 and 3.0 mm aluminum rods in the ratio of 3:2 by weight (Figure 7). The ground is prepared by piling up the stack of aluminum rods from the bottom which results in a unit weight of 20.4 kN/m<sup>3</sup>. This setup simulates a plane strain condition in model tests. Samples of this material have been tested in biaxial tests under constant lateral and axial stress of 19.6 kPa and the results are presented in Figure 8 and 9, respectively.



Figure 7. Material used in 2D model tests (Nakai 2013)

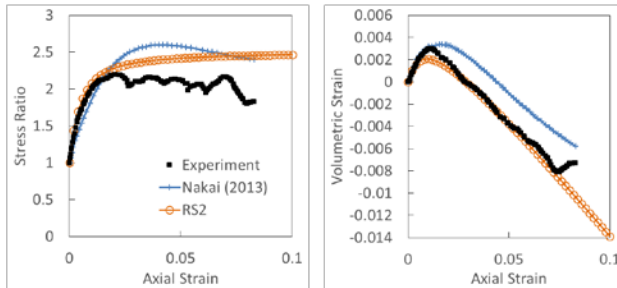


Figure 8. Biaxial test results under constant lateral stress of 19.6 kPa

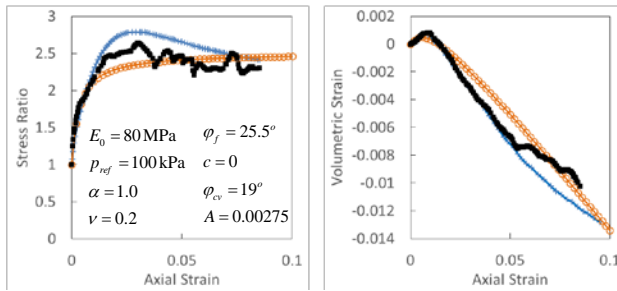


Figure 9. Biaxial test results under constant axial stress of 19.6 kPa

The material properties are included in Figure 9. The stress ratio in Figures 8 and 9 is defined as the ratio of the major principal stress to the minor principal stress. For this case a nonlinear elastic behaviour is considered for the material. This is one of the flexibilities of the proposed model that can take advantage of nonlinear elastic behaviour in addition to its simple deviatoric hardening rule. The nonlinear elastic behaviour is presented in Equation 9 on the basis that the elastic modulus is dependent on the mean stress

$$E = E_0 \left( p / p_{ref} \right)^\alpha \quad [9]$$

where  $p_{ref}$  is the reference pressure,  $E_0$  is the elastic modulus at reference pressure and  $\alpha$  is the exponent constant.

The numerical results presented by Nakai (2013) are based on a more complex formulation than the constitutive model proposed in this work.

The model test that is studied here is a tunnel with a nearby surface load from a rigid footing. A simple bearing capacity analysis is also conducted to evaluate the bearing capacity of the foundation. Another simple analysis is performed to examine the effects of excavation solely. The schematic 2D test setup is presented in Figure 10. For details of the testing setup readers are referred to Shahin et.al (2011) and Nakai (2013).

The ground model is 80cm wide with 40cm depth. The in-situ vertical stress is due to gravity and the ratio of horizontal stress to vertical stress was measured to be 70%. The rigid footing is made of steel plate that is 8cm wide and has 1cm thickness. The vertical load is applied at the center line of the footing and is equal to  $Q_v = 0.32 \times 9.81 \text{ N/cm}$ . The diameter of the tunnel is 10cm, and the depth to diameter ratio is  $D/B = 2.0$  (Figure 10). The excavation is simulated by a special device that controls the displacements on the boundary of the tunnel. As a result of excavation it is assumed that circular shape of the tunnel will be preserved and the diameter will shrink while the invert of the tunnel is fixed. The tunnel displacement pattern is illustrated in Figure 11. For the model test the tunnel displacement is  $d_c = 4\text{mm}$ .

The result of the bearing capacity analysis is presented in Figure 12. There is close agreement between the observed behaviour and the numerical results produced by the proposed model. For comparison the numerical results from Nakai (2013) are also presented.

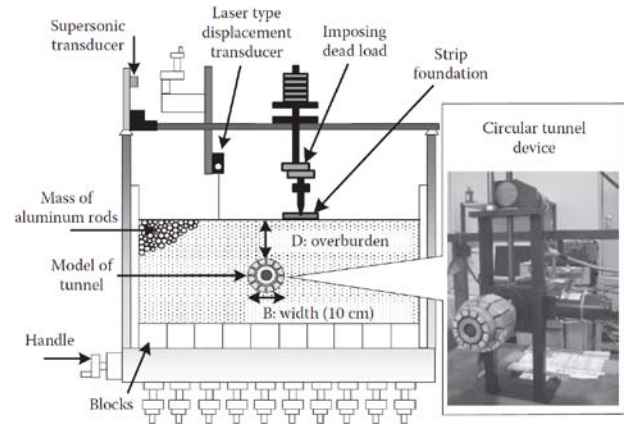


Figure 10. Schematic diagram of the 2D model tests (Nakai 2013)

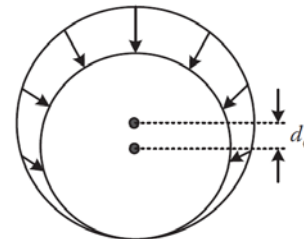


Figure 11. Displacement pattern of the excavated tunnel with fixed invert (Nakai 2013)

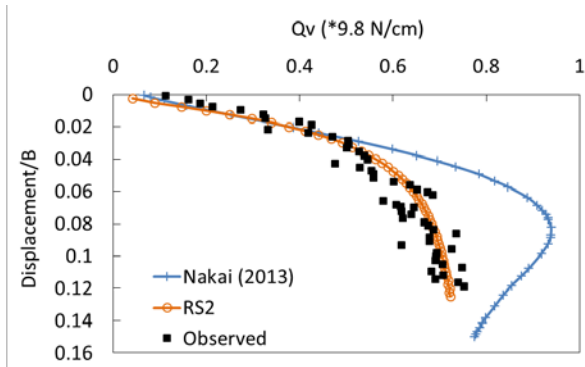


Figure 12. Results of the bearing capacity analysis

The results of the model test experiment and simulations are presented in Figures 13 and 14. Figure 13 shows the surface settlement. The results are presented for the case of greenfield (no surface load) and nearby surface load. The numerical results are in good agreement with the experiments. An interesting observation in the model test is that the maximum settlement occurs under the footing at the edge that is farther from the tunnel. This is well captured in the numerical simulations by Nakai (2013) and the present study. Conducting an elastic analysis or an elasto-perfect-plastic analysis using the Mohr-Coulomb model will predict the maximum settlement at the edge that is closer to the tunnel.

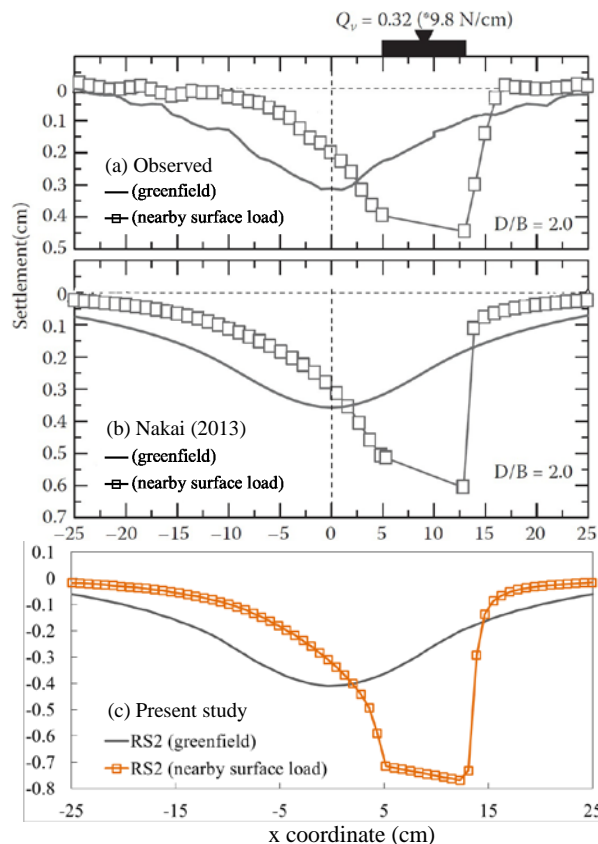


Figure 13. Surface settlement profile with and without nearby surface load

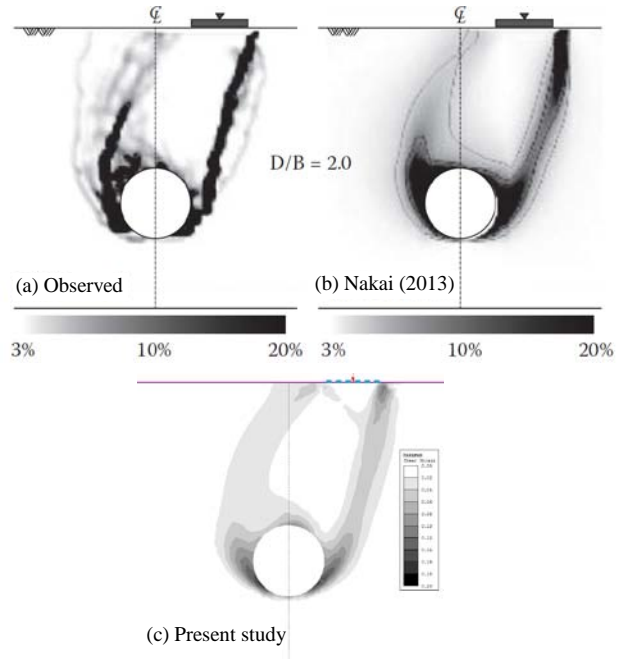


Figure 14. Distribution of deviatoric strain; a) observed behaviour, b) numerical simulation results after Nakai (2013), c) numerical simulation results present study

The distribution of deviatoric strain in the domain can be used to analyse the failure modes. Concentration of high deviatoric strains is an indication of formation of shear bands, failure and slip surfaces. Figure 14 shows the distribution of deviatoric strain in the domain of the model test. There is a good agreement between the observed pattern and the contours plots from the numerical simulations.

### 3.3 Anchored Diaphragm Wall in Berlin Sand

The final numerical simulation is the problem described in Schweiger (2002). This benchmark problem has been studied and analyzed numerically by many researchers (e.g. Schweiger 2002 and Nikolinakou et. al 2011), and also is cited by most of the commercially available finite element (e.g. PLAXIS 2014) or finite difference packages (FLAC 2011) as a verification problem.

The geometry, basic assumptions, groundwater condition and stages of excavations are taken from the benchmark problem described in Schweiger (2002) and summarised in Figure 15. The soil profile consists of three different layers of sands. The stages of the analysis are:

- 1- Initializing the in-situ stress state and groundwater condition. The  $K_0$  condition for sand 1 is 0.43 and for sand 2 and sand 3 is 0.38. The ground water is initially at depth 3m.
- 2- The diaphragm wall is put in place and water table in the excavated area is lowered to 17.9m depth.
- 3- Excavation of step 1 to 4.8m depth.
- 4- Installation of the first row of anchors at 4.3m depth.
- 5- Excavation of step 2 to 9.3m depth.

- 6- Installation of the second row of anchors at 8.8m depth.
- 7- Excavation of step 3 to 14.35m depth.
- 8- Installation of the third row of anchors at 13.85m depth.
- 9- Excavation of step 4 to 16.8m depth

The density of the of the diaphragm wall is 2400 kg/m<sup>3</sup> with a Young's modulus of 30 GPa and Poisson's ratio of 0.15. The wall is 80cm thick. The cross section area of anchors is 15cm<sup>2</sup> and their Young's modulus is 210 GPa. Other properties of the anchors are given in Table 1.

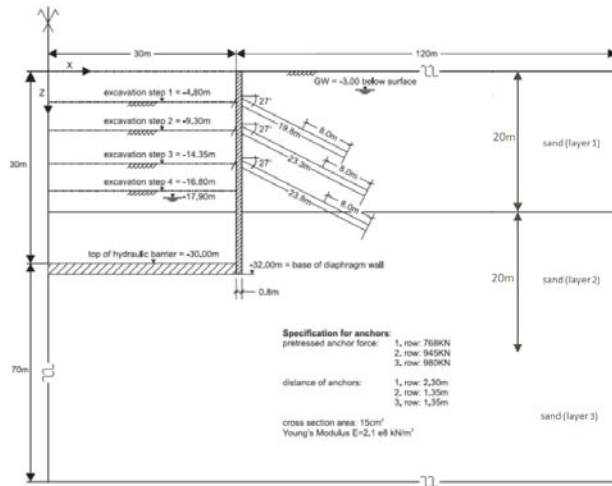


Figure 15. Geometry and excavation stages (after Schweiger 2002)

Table 1. Anchors Specifications

Characteristics	Row 1	Row 2	Row 3
Depth (m)	4.8	9.3	14.35
Dip angle (degrees)	27	27	27
Total length (m)	19.8	23.3	23.8
Bond length (m)	8	8	8
Out of plane spacing (m)	2.3	1.35	1.35
Pre-tensioning force (kN)	768	945	980

To identify the material properties a series of drained and undrain triaxial test simulations were performed using the Hardening Soil model and the material properties given in PLAXIS manual (2014). The material properties used in the Hardening Soil model and the simulated triaxial test results were then used to determine the model parameters of the proposed constitutive model. The material properties of the three different layers of Berlin sand are given in Table 2, 3 for the Hardening Soil model and the proposed constitutive model, respectively. The unit weight of all sands is 19 kN/m<sup>3</sup>.

Comparing Table 2 and 3, it is clear that the elastic properties are transferred directly from the Hardening Soil model to the proposed model, assuming that  $E_0 = E_{50}^{ref}$ . The friction angle and cohesion are the same and the critical friction angle is equal to the friction angle minus

the dilation angle. The hardening parameter is identified using the generated triaxial test results and the curve fitting process explained as in Figure 3.

The simulated triaxial test results are presented in Figures 16 to 21. It is worth mentioning once again that the simulation results generated by the Hardening Soil model with the properties listed in Table 2 are the basis for identification of material parameters in Table 3. Comparisons between the two series of simulated triaxial test results in Figures 16 to 21 show a close agreement between the predicted mechanical behaviours of Berlin sands.

After the verification of material parameters in Table 3 they are used in the simulation of the anchored diaphragm wall in Berlin sand as described in Figure 15. The results of this simulation are presented in terms of the wall deflection at the final stage of excavation in Figure 22.

Table 2. Hardening Soil model parameters for three sand layers of Berlin excavation problem (PLAXIS 2014)

Characteristics	Row 1	Row 2	Row 3
$p_{ref}$ (kPa)	100	100	100
$E_{50}^{ref}$ (MPa)	45	75	105
$E_{ur}^{ref}$ (Ma)	180	300	315
$E_{ocd}^{ref}$ (MPa)	45	75	105
$m$	0.55	0.55	0.55
$\nu$ (Poisson's ratio)	0.2	0.2	0.2
$G_0^{ref}$ (MPa)	168.75	281.25	-
$\gamma_{0.7}$	0.0002	0.0002	-
$K_0^{nc}$	0.43	0.38	0.38
$\phi$ (degrees)	35	38	38
$\psi$ (degrees)	5	6	6
$c$ (kPa)	1.0	1.0	1.0
Failure ratio	0.9	0.9	0.9
Tensile strength (kPa)	0	0	0

Table 3. Material parameters of the proposed constitutive model for three sand layers of Berlin excavation problem

Characteristics	Row 1	Row 2	Row 3
$p_{ref}$ (kPa)	100	100	100
$E_0$ (MPa)	45	75	105
$m$	0.55	0.55	0.55
$\nu$ (Poisson's ratio)	0.2	0.2	0.2
$\phi$ (degrees)	35	38	38
$\phi_{cv}$ (degrees)	30	32	32
$c$ (kPa)	1.0	1.0	1.0
$A$	0.0005	0.0004	0.0003
Tensile strength (kPa)	0	0	0

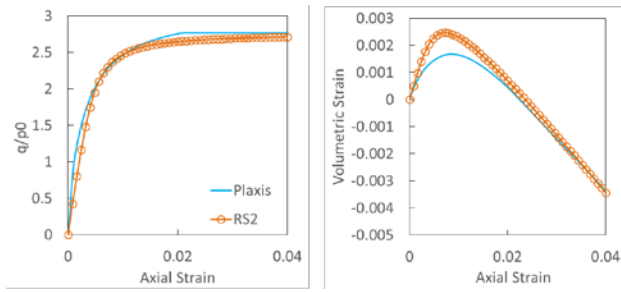


Figure 16. Simulated behaviour of Sand 1 in drained triaxial compression test (initial confinement 50 kPa)

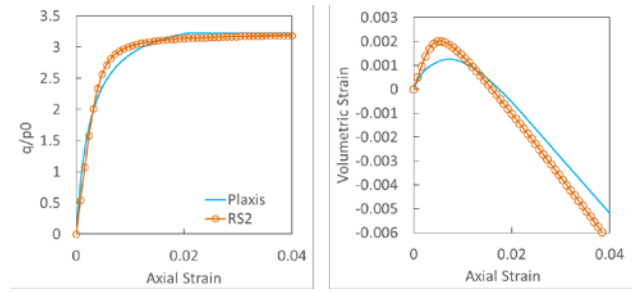


Figure 20. Simulated behaviour of Sand 3 in drained triaxial compression test (initial confinement 200 kPa)

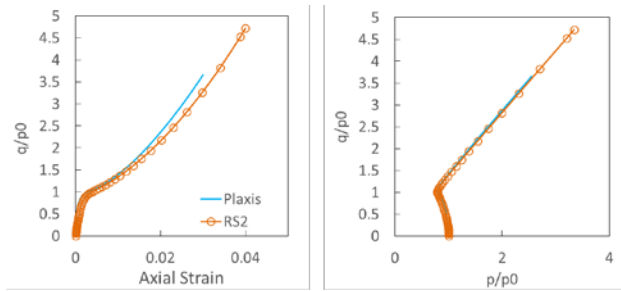


Figure 17. Simulated behaviour of Sand 1 in undrained triaxial compression test (initial confinement 50 kPa)

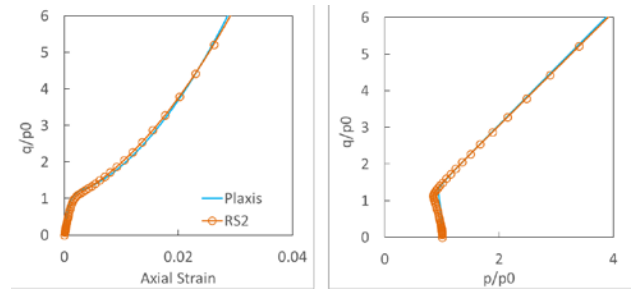


Figure 21. Simulated behaviour of Sand 3 in undrained triaxial compression test (initial confinement 200 kPa)

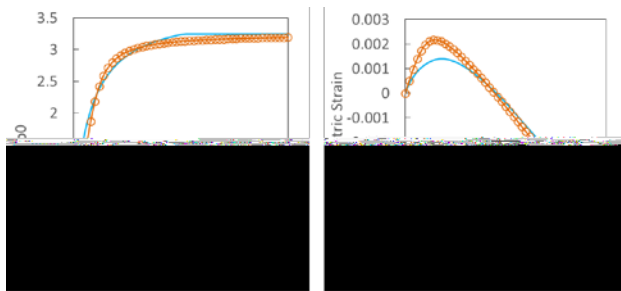


Figure 18. Simulated behaviour of Sand 2 in drained triaxial compression test (initial confinement 100 kPa)

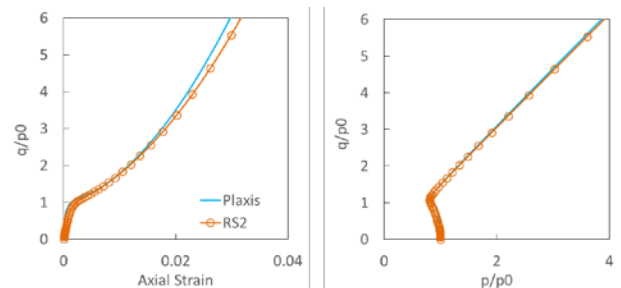


Figure 19. Simulated behaviour of Sand 2 in undrained triaxial compression test (initial confinement 100 kPa)

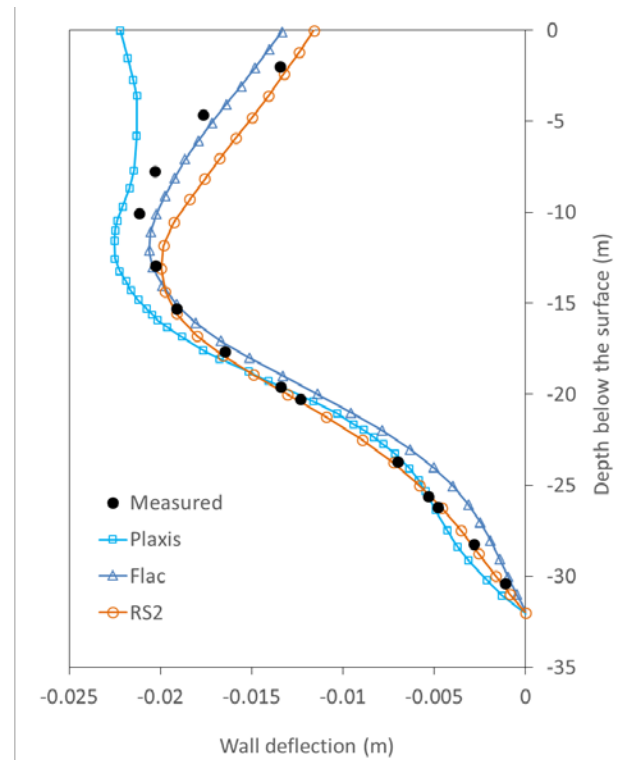


Figure 22. Wall deflection at the final stage of excavation.

For comparison, the numerical results presented in PLAXIS manual (2014) and FLAC manual (2011) for the same problem are included in Figure 22.

The numerical simulation results presented for this benchmark problem (Schweiger 2002) show that the predictions of wall deflection are not accurate for the cases where a nonlinear elastic model or an elasto-perfect-plastic model is used to model the Berlin sand behaviour. To accurately simulate this problem the major aspects of the sands behaviour should be addressed in the constitutive equations.

By looking at Tables 2 and 3 it can be seen that the proposed model requires fewer model parameters to simulate the same problem accurately when compared to Hardening Soil (Plaxis 2014) model. The choice of right constitutive model for the type of materials included in a problem is a major key factor for the success of a numerical simulation. The proposed model can capture the major features of the mechanical behaviour of sands with a minimum number model parameters.

#### 4 CONCLUSIONS

The main objective of this paper was to propose a simple yet practical material model for granular materials under monotonic loading. Major features of the mechanical behaviour of sands under loads are their deviatoric hardening and volumetric behaviour that is mostly dependent on the material density.

The deviatoric hardening model presented in this work is based on the Mohr-Coulomb model which is the most common constitutive model applied to soils. It takes advantage of the same material properties, cohesion and friction angle in addition to one essential model parameter. An optional flow rule is also considered to better capture the volumetric behaviours.

The validity and applicability of the model were demonstrated in various simulations of triaxial tests, model tests, and a practical geotechnical boundary value problem.

#### REFERENCES

- Castro, G. 1969. Liquefaction of sands, *Harvard Soil Mechanics Series*, No.81, Pierce Hall.
- Duncan, J.M. and Chang, C.Y. 1970. Nonlinear analysis of stress and strain in soils. *J. of Soil Mech. and Foundation Division*, ASCE, 96 (SM5): 1629-1653.
- FLAC, *Constitutive Models Manual*, Itasca Consulting Group, Minnesota, USA, 2011.
- Nakai, T. 2013. *Constitutive modeling of geomaterials, principles and applications*, CRS Press.
- Nikolinakou, M.A., Whittle, A.J., Savidis S., and Schran, U. 2011. Prediction and interpretation of the performance of a deep excavation in Berlin sand. *ASCE Journal of Geotechnical and Geoenvironmental Engineering*, 137(11): 1047-1061
- Pietruszczak, S. 2010. *Fundamentals of Plasticity in Geomechanics*, Leiden, The Netherlands: CRC Press.
- PLAXIS, *Material Models Manual*, Delft, Netherlands, 2014.

- Rowe, P.W. 1962. The stress-dilatancy relation for static equilibrium of an assembly of particles in contact, *Proc. Roy. Soc. A* 269, 500-527.
- Rocscience, *RS<sup>2</sup> (Phase<sup>2.9</sup>) Manual*, Toronto, Canada 2015.
- Schanz, T. and Vermeer, P.A. 1996. Angles of friction and dilatancy of sand, *Géotechnique* 46(1): 145-151.
- Schweiger, H.F. 2002. Results from numerical benchmark exercises in geotechnics. *5th European Conference Numerical Methods in Geotechnical Engineering pp. 305-314*, Numge, Paris, Vol. 1.
- Shahin, H. M., Nakai, T., Zhang, F., Kikumoto, M. and Nakahara, E. 2011. Behaviour of ground and response of existing foundation due to tunneling, *Soils and Foundations*, 51(3): 395-409.